DOI:10.11835/j.issn.2096-6717.2020.125 开放科学(资源服务)标识码(OSID):

Numerical modeling of flanged RC shear walls considering shear deformation and coupled flexural-shear effects

ZHANG Pinle, HE Yaoqiong, ZHANG Gan, LIU Junxiong, ZHANG Zhiji

(Department of Civil Engineering, Kunming University of Science and Technology, Kunming 650500, P. R. China)

Abstract: A new flexibility-based nonlinear finite element model that considers shear deformation and coupled flexural-shear effects is proposed in this article. Cyclic loading tests of T-shaped and L-shaped shear wall specimens were conducted to verify the validity of the proposed model. All specimens exhibited a flexural failure mode characterized by the crushing of the concrete and the buckling of the reinforcement at the free web boundary. Closer stirrups and longer confined boundary elements should be used in the free web end to prevent premature failure when compressed. The seismic design of the boundary element at the web-flange junction could be relaxed, as no concrete spalling was observed at the web-flange junction. The ductility decreased as the shear span ratio decreased. The specimens exhibited higher strength and stiffness but lower ductility when the flange was in tension. Numerical simulation of the cyclic loading test of the RC flanged shear wall was conducted based on the proposed model, demonstrating that the model efficiently simulates the nonlinear response of RC flanged shear walls, as proved by satisfactory agreement between the analytical results and the test results.

Keywords: shear wall; quasi-static test; fiber model; shear deformation; coupled flexural-shear effects

考虑剪切变形和弯剪相互作用的带翼缘剪力墙数值模型

张品乐,何尧琼,张淦,刘俊雄,张智吉

(昆明理工大学 建筑工程学院,昆明 650500)

摘 要:提出了一种基于柔度法的考虑剪切变形和弯剪耦合效应的有限元模型,通过 T 形和 L 形剪力墙试件拟静力试验验证了模型的正确性。结果表明,所有试件的破坏形态为无翼缘腹板端部混凝土压碎、纵筋压曲的弯曲破坏;增强无翼缘腹板端部约束和边缘构件约束,可以防止其发生受压过早破坏;腹板和翼缘相交处未观察到明显的混凝土剥落现象,腹板和翼缘相交处的约束边缘构件抗震设计可以适当放宽;随着剪跨比的减小,试件延性明显降低;当翼缘处于受拉时,试件表现出较高的强度、刚度和较低的延性。基于模型对钢筋混凝土带翼缘剪力墙的拟静力试验进行了非线性数值模拟分析,分析结果与试验结果吻合较好,表明模型能较好地模拟钢筋混凝土带翼缘剪力墙的非线性性能。

关键词:剪力墙;拟静力试验;纤维模型;剪切变形;弯剪相互作用

中图分类号:TU398.2 **文献标志码**:A **文章编号**:2096-6717(2021)01-0145-10

Received:2020-04-15

Foundation item:National Natural Science Foundation of China (No: 51568028)

Author brief:ZHANG Pinle (1975-), associate professor, PhD, main research interest: concrete structure, E-mail: zhangpinle@aliyun.com.

1 Introduction

Reinforced concrete walls are effective in resisting lateral loads placed on high-rise buildings[1]. They provide enough strength and deformation capacity to meet the demands of strong earthquake ground motions[2-4] A great deal of research has been performed to investigate the seismic behavior of RC walls[5-8]. Previous tests have been conducted on either rectangular shear walls or flanged shear walls with ordinary strength reinforcement. However, this paper focuses on the experimental study of the seismic behavior of flange RC shear walls with high strength stirrups. Six flanged RC shear wall specimens with high strength stirrups were tested to failure under cyclic loading. The effects of the axial load ratio, aspect ratio, and confinement on the failure mode, ductility capacity, hysteretic behavior, and energy dissipating capacity were investigated.

Simulation of the nonlinear response of RC shear walls requires the use of a reliable computational model. Two-dimensional continuum plane stress or shell elements are usually used for this purpose, but such elements are computationally expensive. Previous studies have shown that beam-column elements can be used to simulate the nonlinear behavior of RC shear walls[9-10] In regards to this, much research has emerged in recent decades in the field of stiffness-based fiber beam-column elements[11-12]. So far, most stiffness-based element models become less accurate in highly nonlinear situations, since the displacement field is approximated through the assignment of the displacement interpolation function. In most cases, cubic Hermitian polynomials are used for the displacement interpolation functions. Simple numerical examples presented indicate that the conventional displacement formulation is unable to establish solutions associated with softening behavior, when used at the section or member level. This problem can be solved with the use of more elements per member; however, this leads to much less efficiency. Most efforts in the nonlinear analysis of RC structures have demonstrated that flexibility-based element methods offer greater accuracy and computational efficiency[13], since the element formulations satisfy the equilibrium of the bending moment, the axial force and the shear force along the element[14-15].

Shear deformation accounts for a large portion of the total deformation of flanged RC shear walls under lateral loading. Flexibility-based finite element methods ignore the effect of shear deformation, which is suitable for slender RC members but less applicable to shear walls with small slenderness ratios. A flexibility-based nonlinear finite element model that considers shear deformation and coupled flexural-shear effects, which offers greater accuracy and computational efficiency, since fewer elements are needed along the length of the member, is proposed in this study. Furthermore, cyclic loading tests of flanged shear wall specimens are carried out to validate the analytical results. Lastly, seismic behaviors of flanged RC walls are summarized, and key issues related to seismic design are discussed.

2 Fiber element model

The fiber element model is shown in Fig. 1. The RC shear wall is divided into many cross sections along the vertical direction, and every cross section is divided into many reinforcement and concrete fibers along the horizontal direction. Each fiber is characterized by its cross-section area and its basic uniaxial nonlinear stress-strain relationship for concrete and reinforcement. Element degrees of freedom (DOFs) are shown in Fig. 2.

The element force vector and displacement vector are denoted by the first two equations

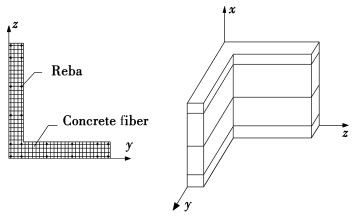

Fig. 1 Fiber element model

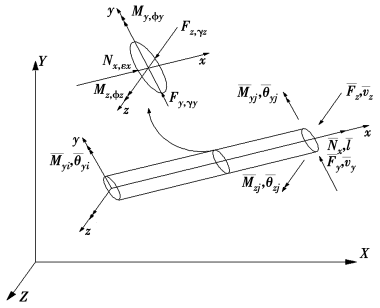

Fig. 2 Element degree of freedom without rigid-body modes

$$\{\bar{F}\}^{e}=[\bar{M}_{yj}\quad \bar{M}_{yi}\quad \bar{M}_{zj}\quad \bar{M}_{zi}\quad \bar{F}_{y}\quad \bar{F}_{z}\quad \bar{N}_{x}]^{T} \tag{1}$$

$$\{\bar{d}\}^{e}=[\bar{\theta}_{yj}\quad \bar{\theta}_{yi}\quad \bar{\theta}_{zj}\quad \bar{\theta}_{zi}\quad \bar{\nu}_{y}\quad \bar{\nu}_{z}\quad \bar{l}]^{T} \tag{2}$$

The section force and the corresponding section deformation are respectively denoted as

$$\{F(x)\}^{s}=M_{y}(x)\quad M_{z}(x)\quad F_{y}(x)\quad F_{z}(x)\quad N_{x}(x)]^{T} \tag{3}$$

$$\{d(x)\}^{s}=[\varphi_{y}(x)\quad \varphi_{z}(x)\quad \gamma_{y}(x)\quad \gamma_{z}(x)\quad \varepsilon_{x}(x)]^{T} \tag{4}$$

where $M_y(x)$ and $M_z(x)$ are the bending moment about the y-axis and the z-axis, respectively; $F_y(x)$ and $F_z(x)$ are the shear force in the y and z direction, respectively; $N_x(x)$ is the sectional axial force; $\varphi_y(x)$ and $\varphi_z(x)$ are the curvature about the y-axis and z-axis, respectively; $\gamma_y(x)$ and $\gamma_z(x)$ are the shear deformation in the y and z direction, respectively; $\varepsilon_x(x)$ is the axial deformation.

The section force $\{F(x)\}^{s}$ can be interpolated from the element nodal force $\{\bar{F}\}^{e}$ according to the following equation,

$$\{F(x)\}^{s}=N_{f}(x)\ \{\bar{F}\}^{e} \tag{5}$$

Where $N_f(x)$ is the force interpolation matrix given by

$$N_{f}(x)=\begin{bmatrix}-(1-\frac{x}{L}) & \frac{x}{L} & 0 & 0 & 0 & 0 & 0\\ 0 & 0 & -(1-\frac{x}{L}) & \frac{x}{L} & 0 & 0 & 0\\ 0 & 0 & 0 & 0 & 1 & 0 & 0\\ 0 & 0 & 0 & 0 & 0 & 1 & 0\\ 0 & 0 & 0 & 0 & 0 & 0 & 1\end{bmatrix} \tag{6}$$

The section constitutive relation can be denoted as

$$\mathrm{d}\{d(x)\}^{s}=[f(x)]^{s}\mathrm{d}\{F(x)\}^{s} \tag{7}$$

where $\{f(x)\}^{s}$ is the section tangent flexibility matrix.

Using the principle of virtual force, Eq. (5) and Eq. (7) give

$$[f]^{e}\mathrm{d}\{F\}^{e}=\mathrm{d}\{d\}^{e} \tag{8}$$

where $[f]^{e}$ is the element flexibility matrix.

$$[f]^{e}=\int_{L}[N_{f}(x)]^{T}[f(x)]^{s}[N_{f}(x)]\mathrm{d}x \tag{9}$$

Element stiffness matrix $[k]^{e}$ can be obtained by the inversion of the element flexibility matrix

$$[k]^{e}=[[f]^{e}]^{-1} \tag{10}$$

3 Constitutive relation of fiber material

3.1 Axial constitutive relation of fiber

Nonlinear characteristics of the fiber element model are mainly governed by the constitutive relation of the fiber material. The uniaxial constitutive relation of materials is used for the axial constitutive relation of the fiber. In this paper, the reinforcement constitutive model proposed by Hoehler and Stanton[16], is selected, as shown in Fig. 3. The concrete constitutive model proposed by Hoshikuma[17] is used. The concrete hysteretic rule proposed by Mander[18] is selected, as shown in Fig. 4.

3.2 Shear stiffness of fiber

It is assumed that the reinforcement is dispersed into the concrete, and the two materials act together to resist the shear force. Thus, only the shear stiffness of the concrete fiber is considered and the shear stiffness of the reinforcement fiber is not considered. For each

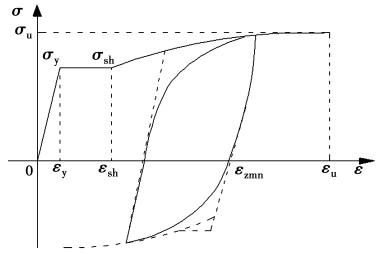

Fig. 3 Reinforcement constitutive model

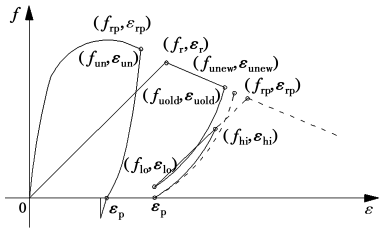

Fig. 4 Concrete hysteretic rule

concrete fiber, the shear stiffness is determined by its different axial stress state. The detailed calculation methods are listed below:

1) It is assumed that the elastic shear stiffness of the fiber is G_e, when the fiber is compressed. The shear stiffness of the fiber is r_1G_e, when the compressive strain of the fiber reaches the yield strain of the reinforcement. The shear stiffness of the fiber is r_2G_e, when the compressive strain of the fiber reaches or exceeds the peak strain of the concrete.

2) The shear stiffness of the fiber is r_3G_e, when the tensile strain of the fiber reaches the cracking strain of the concrete. The shear stiffness is r_4G_e, when the tensile strain of the fiber reaches the yield strain of the reinforcement. The shear stiffness is r_5G_e, when the tensile strain of the fiber reaches or exceeds the ultimate tensile strain of the reinforcement.

The shear stiffness of the fiber between the two states can be obtained by interpolation. According to the latest research, $r_1=0.5$, $r_2=0.02$, $r_3=0.5$, $r_4=0.15$ and $r_5=0.02$[19].

4 Experiment details

4.1 Specimen design and loading program

In order to verify the fiber element model of flanged RC shear walls proposed in this study, six RC flanged shear wall specimens, named L500, L650, L800, T500, T650 and T800 respectively, were tested under cyclic loading. The vertical height of the walls was 1 400 mm, and their cross-section thickness was 100 mm. The design strength grade of the concrete was C40 (nominal cubic compressive strength $f_{cu,k}=40$ MPa). The test average cubic compressive strength f_{cu} of the concrete measured on cubes of 150 mm size was 47.2 MPa. The mechanical properties of the reinforcement are shown in Table 1. Specimen details and properties are summarized in Table 2, where the steel ratio ρ_s of the longitudinal reinforcement is defined as the ratio of the cross sectional area of the longitudinal reinforcement to the total wall cross sectional area, and the volumetric steel ratio ρ_v of the boundary element at the non-flange end is defined as the ratio of the volume of the stirrups to that of the wall (Chinese GB 50010-2010 code)[20]. Dimensions and reinforcement details of the specimens are shown in Fig. 5.

Table 1 Yield and ultimate stresses of the reinforcement of the shear wall

Steel type	Yield stress/ (N·mm^{-2})	Ultimate stress/ (N·mm^{-2})	Elongation/ %	Elastic modulus/ (N·mm^{-2})
#4 Rebar	730	985	8	205 000
#8 Rebar	295	510	28	210 000
#12 Rebar	345	600	31	216 000

Table 2 Properties of specimens

Specimens	Cross-section height to width ratio	ρ_v/ %	ρ_s/ %	Aspect ratio	Axial load/kN
L500	5.0	0.62	1.95	2.80	554.4
L650	6.5	1.25	1.71	2.15	739.2
L800	8.0	0.58	1.74	1.75	924.0
T500	5.0	0.81	1.95	2.80	554.4
T650	6.5	0.81	1.71	2.15	739.2
T800	8.0	0.58	1.74	1.75	924.0

The axial load was first applied to the center of the shear wall by the vertical jack, and kept

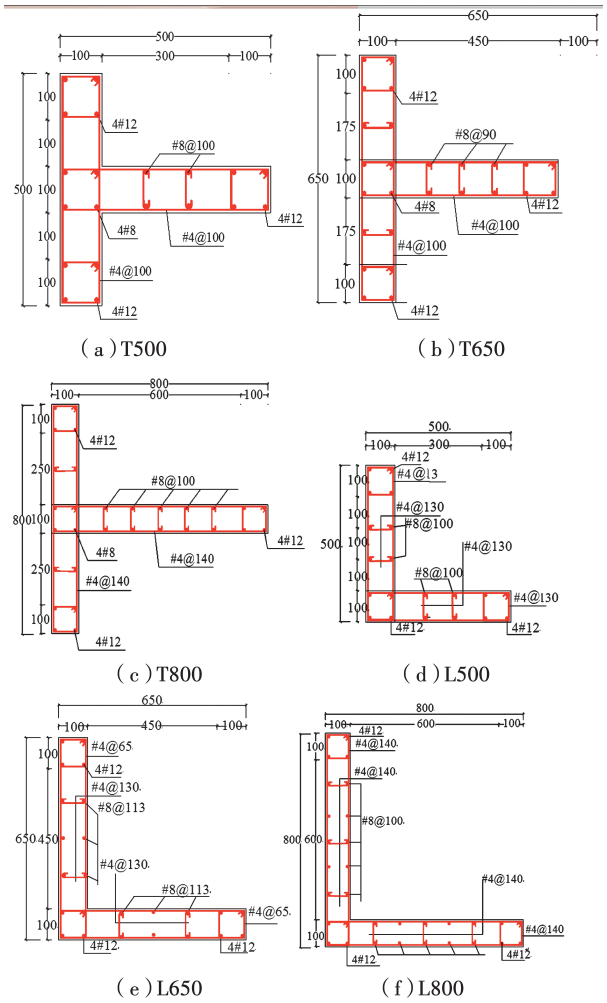

Fig. 5 Dimensions and reinforcement details of RC shear wall specimens(mm)

constant during the test. Fig. 6 shows the test setup including loading devices. The scheme of the loading program is shown in Fig. 7. The loading history was started by applying two identical displacement cycles with increments of ±2 mm up to 10 mm, followed by increments of ±5 mm up to failure. Each test continued until the specimens dropped to 85% of the peak lateral load.

4.2 Damage development and failure mode

In this experiment, all specimens exhibited a flexural model characterized by the crushing of the concrete and the buckling of the reinforcement at the free web boundary, as shown in Fig. 8. During the test, flexural cracks were first observed at the bottom of the web when the specimens were loaded to approximately half the peak lateral load. Shear cracks began to form at a drift level of 0.4%. As

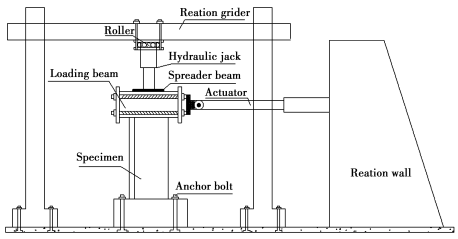

Fig. 6 Test setup

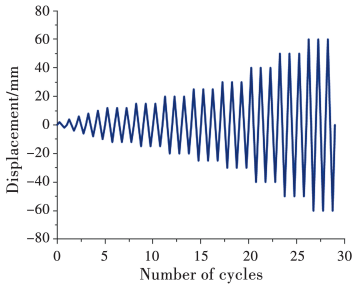

Fig. 7 Loading history

the loading displacement increased to a drift level of 1.3%, vertical splitting of the free web was quite extensive, and severe crushing and spalling of the concrete cover were observed. As the loading displacement increased to a drift level of 3.0%, major crushing of the concrete occurred, and the outermost longitudinal reinforcing bars started to buckle. The lateral force dropped to 85% of the peak lateral load. The failure mechanism suggested that closely spaced stirrups and longer confined boundary elements should be used in the free web end, preventing premature failure under compression. No obvious concrete spalling was observed at the web-flange junction, suggesting that the seismic design of the boundary element at the web-flange junction should be relaxed.

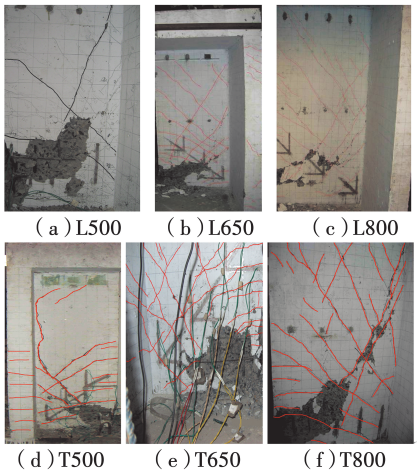

Fig. 8 Crack patterns and failure of specimens

4.3 Loading capacity and ductility

The loading capacity and displacement ductility of the shear wall specimens are shown in Table 3. As shown, the specimens exhibited bigger loading capacity but lower ductility capacity when the flange was in tension. With the decrease of the shear span ratio, the displacement ductility decreased. The smaller the shear span ratio, the closer the stirrups and the longer the confined boundary elements should be used in the free web end to achieve the goal of the displacement ductility coefficient of 3.0. For example, specimens T800, L800. The ductility in the negative position of T800, L800 were, 2.2, 1.9, respectively, meaning that the volumetric steel ratio of the boundary element (0.60%) was not enough for specimens T800 and L800 with the aspect ratio of 1.75. The use of high strength stirrups could restrain the compressed concrete and postpone the buckling of the longitudinal rebars in the free web boundary, preventing premature failure when the web was compressed. The ultimate drift ratio of all specimens greatly exceeded the allowable inter-story drift ratio value (1/120) of the RC shear wall according to the design provisions of the Chinese GB 50011-2010 code[21].

Table 3 Loading capacity and ductility

Specimen	Δ_c/mm	F_c/kN	Δ_y/mm	F_y/kN	Δ_m/mm	F_m/kN	Δ_u/mm	F_u/kN	μ	θ_u
T500	3.2	60.2	8.4	93.5	27.7	117.5	35.1	111.2	4.2	1/39.9
	−2.5	−84.3	−4.7	−133.5	−12.5	−193.6	−18.3	−163.9	3.9	1/76.5
T650	1.9	80.0	5.5	120.0	17.8	161.1	37.9	153.4	6.9	1/37.0
	−2.5	−124.8	−3.5	−140.0	−16.3	−266.6	−22.5	−239.3	6.4	1/62.2
T800	1.8	160.5	7.5	280.9	21.0	319.5	29.0	312.0	3.9	1/48.3
	−1.8	−207.8	−5.8	−322.4	−11.3	−367.5	−12.8	−312.3	2.2	1/109.4
L500	3.5	82.8	7.3	113.6	19.8	148.5	42.5	131.8	5.8	1/32.9
	−3.9	−80.5	−6.6	−105.7	−21.7	−138.7	−30.1	−122.7	4.6	1/46.5
L650	3.8	120.6	7.1	160.5	22.3	194.5	28.1	184.2	4.0	1/49.8
	−3.9	−140.3	−7.2	−180.5	−20.3	−231.1	−20.1	−231.1	2.8	1/69.7
L800	3.4	163.6	7.6	220.9	12.9	258.1	19.8	228.8	1.9	1/96.6
	−3.2	−180.8	−6.8	−227.6	−8.9	−251.3	−15.6	−215.5	1.9	1/111.1

Note: Δ_c is the lateral displacement when the web concrete first cracked; F_c is the lateral force when the web concrete first cracked; F_y is the yield lateral force; Δ_y is the yield lateral displacement; F_m is the maximum lateral force; Δ_m is the lateral displacement at the maximum lateral force; F_u is the ultimate lateral force; Δ_u is the ultimate top displacement; μ is the displacement ductility coefficient; θ_u is the ultimate drift ratio.

4.4 Strain analysis

Fig. 9 shows the arrangements of the strain gauges of the reinforcement of the shear wall specimens. Fig. 10 and Fig. 11 show the strain evolution process of the longitudinal reinforcements and the stirrups of the shear wall specimens, respectively. As we can see from Fig. 10, the strain distribution of the longitudinal reinforcement at the peak point remained approximately linear, so the plane cross-section assumption can be used for the design of the flanged RC shear wall. The compression strains of the longitudinal reinforcement at the intersection of the web and flange were extremely small, compared with the tensile strains at the free web boundary, indicating that it is not necessary to add special confinement reinforcement to the web-flange intersection. As shown in Fig. 11, the stirrups that yielded were mainly concentrated in the middle and lower parts of the web, meaning that the shear damage was mainly concentrated in the middle and lower parts of the web. All of the high-strength stirrups at the free web boundary

yielded, showing that the use of high strength stirrups at the free web boundary could confine the transverse deformation of the specimens, thus preventing premature failure when the web was compressed.

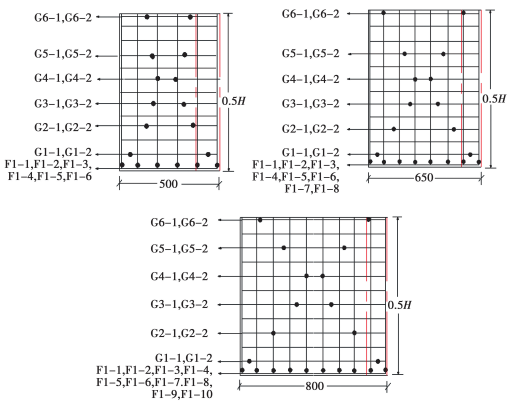

Fig. 9 Arrangement of steel strain gauge

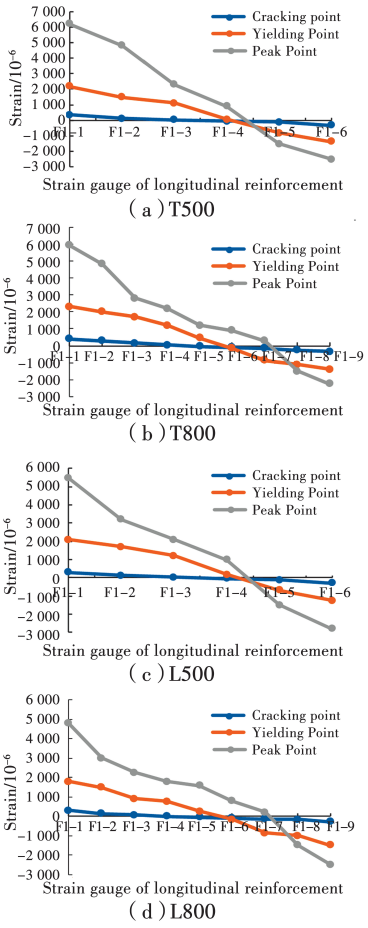

Fig. 10 Strain evolution of the longitudinal reinforcement in the web of the shear wall specimens

4.5 Hysteretic behavior

As shown in Fig. 12, the hysteresis loops of specimens in the positive direction exhibited a much

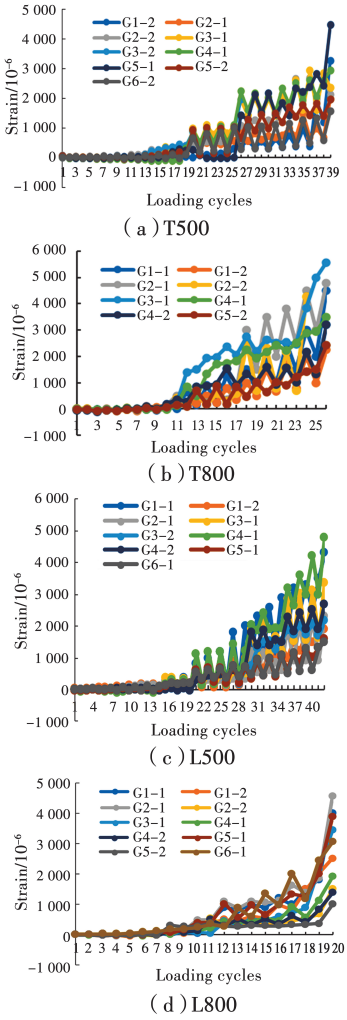

Fig. 11 Strain evolution of the stirrups in the web of the shear wall specimens

wider and thicker shape, showing that higher energy dissipation capacity could be achieved compared with in the negative direction. A pinching effect could be found from the hysteresis loops of specimens in the negative direction for the effect of shear deformation. The hysteresis curves of specimens with a cross-section height-to-width ratio of 6.5 were very plump, and their energy dissipation was very good. The bearing capacity of the T-shaped specimens was greater than that of the L-shaped specimens, because the effective flange width of the T-shaped specimens was bigger than that of L-shaped specimens. Considering the uncertainty of the seismic direction, the seismic performance of the L-shaped shear wall should be far inferior to that of the T-shaped shear wall.

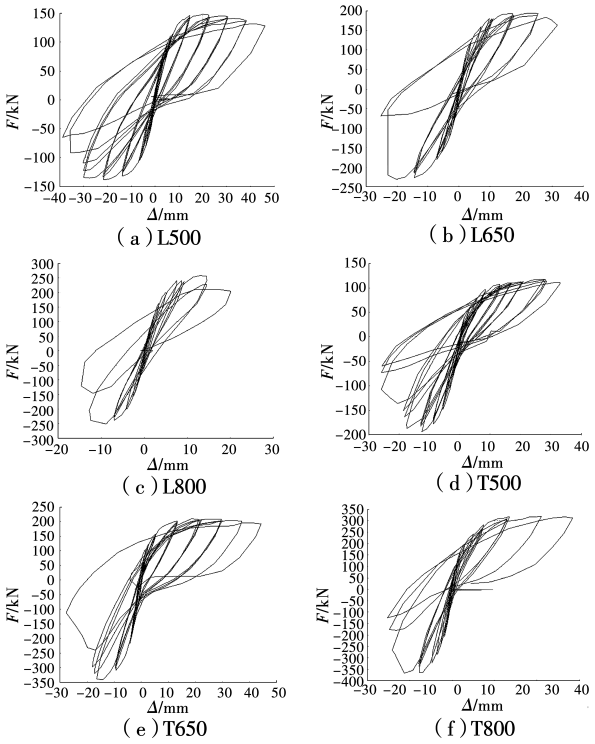

Fig. 12 Force versus displacement hysteresis curves of shear wall specimens

5 Model validation

Shear wall sections are composed of three parts: Cover concrete, core concrete and rebar. Discretization of section fiber is shown in Fig. 13. Section discretization schemes are shown in Table 4. Using a finite analysis program based on the flexibility-based element model that considers shear deformation and coupled flexural-shear effects this paper proposed, numerical analysis of shear wall specimens was carried out to obtain the force-displacement envelopes.

Satisfactory agreement between the analytical results and the experimental results can be seen in Fig. 14. It should be noted that in calculating the ultimate load, the proposed method is approximately 95% of the test results, because the boundary condition on the top of the specimens is fully free in the simulative analysis, but in the test, the vertical jack exerts friction on the top of the specimens. Furthermore, as seen in Fig. 14, the section discretization of various numbers of fibers has little effect on the computational efficiency, since the element formulations strictly enforce force equilibrium.

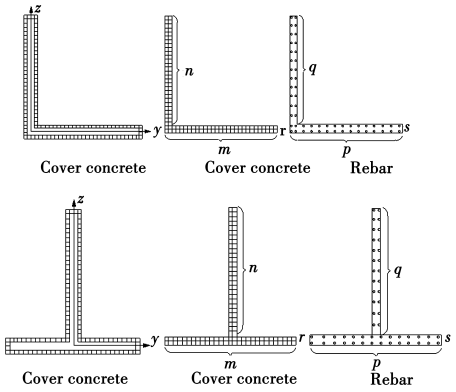

Fig. 13 Discretization of section fiber

Table 4 Section discretization of different numbers of rebar fibers and concrete fibers

Section discretization schemes	*m*	*n*	*r*	*p*	*q*	*s*	Total fiber numbers
SCR1	10	10	2	6	4	2	112
SCR2	40	32	5	8	6	4	581

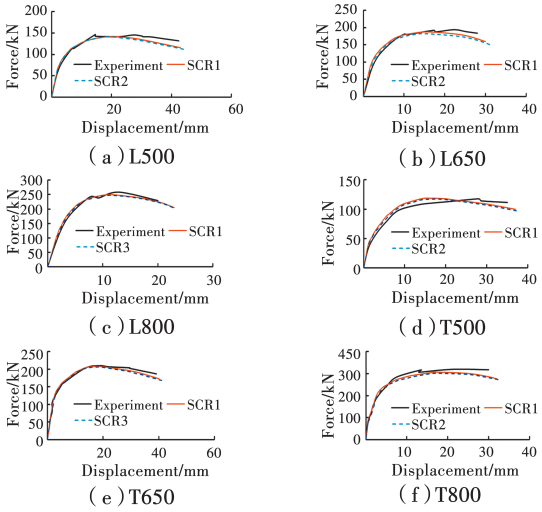

Fig. 14 Force-displacement curves of specimens with different discretizations of section fibers

6 Conclusions

In this paper, a new flexibility-based nonlinear finite element model which considers shear deformation and coupled flexural-shear effects is proposed, and cyclic loading tests of T-shaped and L-shaped shear wall specimens are carried out to verify the proposed model. The following

conclusions can be drawn:

1) All shear wall specimens exhibited a flexural failure model characterized by the crushing of concrete and the buckling of steel at the free web boundary.

2) The use of high strength stirrups could effectively restrain the compressed concrete and postpone the buckling of the longitudinal rebars in the free web boundary, preventing premature failure when the web was compressed. The ultimate drift ratio of all specimens greatly exceeded the allowable inter-story drift ratio value (1/120) of RC shear walls according to the design provisions of the Chinese GB 50011-2010 code.

3) No obvious concrete spalling was observed at the web-flange junction, and the compression strains of the longitudinal reinforcement at the intersection of the web and flange were extremely small, compared with the tensile strains at the free web boundary, indicating that it is not necessary to add special confinement reinforcement to the web-flange intersection.

4) The specimens exhibited higher strength and stiffness but lower ductility capacity when the flange was in tension. The displacement ductility decreased when the shear span ratio decreased. The volumetric steel ratio of the boundary element (0.60%) was not enough for specimens with an aspect ratio under 2.0 to achieve the goal of the displacement ductility coefficient of 3.0.

5) The strain distribution of the longitudinal reinforcement at the peak point remained approximately linear, so the plane cross-section assumption can be used for the design of flanged RC shear walls.

6) A new flexibility-based fiber element model that considered shear deformation and coupled flexural-shear effects was proposed for simulating the nonlinear response of special shaped shear walls, dominated by flexural failure with a small slenderness ratio. There was a good agreement between analytical and experimental results, demonstrating that the model offers excellent accuracy and requires few elements per member, offering a more efficient alternative to the traditional flexibility-based fiber element model in the nonlinear analysis of special-shaped RC shear walls.

Acknowledgements

The authors would like to acknowledge the financial support from the National Natural Science Foundation of China (Grant No: 51568028).

References:

[1] WANG B, SHI Q X, CAI W Z. Seismic behavior of flanged reinforced concrete shear walls under cyclic loading [J]. ACI Structural Journal, 2018, 115(5): 1231-1242.

[2] JI X D, LIU D, QIAN J R. Improved design of special boundary elements for T-shaped reinforced concrete walls [J]. Earthquake Engineering and Engineering Vibration, 2017, 16(1): 83-95.

[3] MA J X, LI B. Seismic behavior of L-shaped RC squat walls under various lateral loading directions [J]. Journal of Earthquake Engineering, 2019, 23(3): 422-443.

[4] ZHANG X M, QIN Y, CHEN Z H, et al. Experimental behavior of innovative T-shaped composite shear walls under in-plane cyclic loading [J]. Journal of Constructional Steel Research, 2016, 120: 143-159.

[5] DING R, TAO M X, NIE X, et al. Analytical model for seismic simulation of reinforced concrete coupled shear walls [J]. Engineering Structures, 2018, 168: 819-837.

[6] REZAPOUR M, GHASSEMIEH M. Macroscopic modelling of coupled concrete shear wall [J]. Engineering Structures, 2018, 169: 37-54.

[7] WU Y T, LAN T Q, XIAO Y, et al. Macro-modeling of reinforced concrete structural walls: state-of-the-art [J]. Journal of Earthquake Engineering, 2017, 21(4): 652-678.

[8] LU X L, YANG J H. Seismic behavior of T-shaped steel reinforced concrete shear walls in tall buildings under cyclic loading [J]. The Structural Design of Tall and Special Buildings, 2015, 24(2)141-157.

[9] MAZARS J, KOTRONIS P, DAVENNE L. A new modelling strategy for the behaviour of shear walls under dynamic loading [J]. Earthquake Engineering & Structural Dynamics, 2002, 31(4): 937-954.

[10] BOLANDER J Jr, WIGHT J K. Finite element modeling of shear-wall-dominant buildings [J]. Journal of Structural Engineering, 1991, 117(6): 1719-1739.

[11] KIM J, LEE S. The behavior of reinforced concrete columns subjected to axial force and biaxial bending [J]. Engineering Structures, 2000, 22(11): 1518-1528.

[12] HAJJAR J F, SCHILLER P H, MOLODAN A. A distributed plasticity model for concrete-filled steel tube beam-columns with interlayer slip [J]. Engineering Structures, 1998, 20(8): 663-676.

[13] ZERIS C A, MAHIN S A. Behavior of reinforced concrete structures subjected to biaxial excitation [J]. Journal of Structural Engineering, 1991, 117(9): 2657-2673.

[14] KILDASHTI K, MIRGHADERI R. Assessment of seismic behaviour of SMRFs with RBS connections by means of mixed-based state-space approach [J]. The Structural Design of Tall and Special Buildings, 2009, 18(5)485-505.

[15] MERGOS P, BEYER K. Modelling shear-flexure interaction in equivalent frame models of slender reinforced concrete walls [J]. The Structural Design of Tall and Special Buildings, 2014, 23(15) 1171-1189.

[16] HOEHLER M S, STANTON J F. Simple phenomenological model for reinforcing steel under arbitrary load [J]. Journal of Structural Engineering, 2006, 132(7): 1061-1069.

[17] HOSHIKUMA J, KAWASHIMA K, NAGAYA K, et al. Stress-strain model for confined reinforced concrete in bridge piers [J]. Journal of Structural Engineering, 1997, 123(5): 624-633.

[18] MANDER J B, PRIESTLEY M J N, PARK R. Theoretical stress-strain model for confined concrete [J]. Journal of Structural Engineering, 1988, 114(8): 1804-1826.

[19] LI H N, LI B. Experimental study on seismic restoring performance of reinforced concrete shear walls [J]. Journal of Build Structures, 2004, 25(5): 35-42.

[20] Code for Design of Concrete Structures: GB 50010-2010 [S]. Beijing: China Architecture & Building Press, 2010.

[21] Code for Seismic Design of Buildings: GB 50011-2010 [S]. Beijing: China Architecture & Building Press, 2010.

(编辑 章润红)